

<sup>1</sup> **The Influence of Leads in Sea Ice on the**  
<sup>2</sup> **Temperature of the Atmospheric Boundary Layer**  
<sup>3</sup> **During Polar Night**

C. Lüpkes,<sup>1</sup> T. Vihma,<sup>2</sup> G. Birnbaum,<sup>1</sup> U. Wacker<sup>1</sup>

---

C. Lüpkes, Alfred Wegener Institute for Polar and Marine Research, Postfach 120161, D-27515  
Bremerhaven, Germany. (Christof.Luepkes@awi.de)

<sup>1</sup>Alfred Wegener Institute for Polar and  
Marine Research, Bremerhaven, Germany

<sup>2</sup>Finnish Meteorological Institute,  
Helsinki, Finland

4 The maximum effect of open leads within sea ice on the near-surface at-  
5 mospheric temperature is estimated using a 1D atmospheric model coupled  
6 with a thermodynamic snow/sea ice model. The study is restricted to clear-  
7 sky conditions during polar night. The model is initialized with a typical win-  
8 tertime atmospheric temperature profile. Results are analyzed at different  
9 integration times corresponding to different fetches over the fractured sea ice  
10 as a function of wind speed and sea ice concentration  $A$ . The results demon-  
11 strate that for  $A > 90$  % small changes in the sea ice fraction have a strong  
12 effect on the near-surface temperature. A change by 1 % causes a temper-  
13 ature signal of up to 3.5 K. A threshold value of about  $4 \text{ m s}^{-1}$  for the 10-  
14 m wind speed divides the air-ice interaction process into a weak-wind and  
15 strong-wind regime.

## 1. Introduction

16 It is essential for climate and weather prediction models that the processes contributing  
17 to the surface energy budget are well represented. Many modeling and observational  
18 studies have been carried out in the past to investigate these processes in polar regions  
19 above sea ice [e.g., *Maykut and Untersteiner, 1971; Ebert and Curry, 1993; Sorteberg et*  
20 *al. 2007*] and it has been shown that one of the most important influencing factors is the  
21 sea ice concentration. However, there is still a large uncertainty on both the observed  
22 and modeled sea ice concentration [*ACIA-report, 2005*]. *Sorteberg et al. [2007]* studied  
23 the Arctic surface energy budget as simulated with 20 different models for the IPCC  
24 (Intergovernmental Panel on Climate Change). They showed that the scatter of modeled  
25 radiative and turbulent fluxes is large (scatter in the turbulent fluxes larger than the  
26 absolute values) with the most significant differences in the marginal sea ice zones, where  
27 the largest differences in the sea ice fraction were found.

28 In the present work, we investigate the dependence of modeled atmospheric boundary  
29 layer temperature (ABL) on the sea ice concentration in polar regions. We restrict our  
30 study to the cold season during polar night, when we can expect strong convection above  
31 leads. For simplicity, we only consider clear-sky conditions keeping in mind, however,  
32 that one important factor influencing the ABL energy budget is without any doubt the  
33 cloud cover [e.g., *Curry et al., 1995*]. The lead effect is, however, largest under clear  
34 skies in winter, when the surface temperature difference between open leads and thick,  
35 snow-covered sea ice can be up to 40 K. Accordingly, the present investigation neglecting  
36 clouds represents an estimation of the maximum possible impact of leads. Note also, that

37 cloud-free days occur quite often during arctic winter (e.g., 27 % of all days during the  
38 SHEBA ice camp [*Mirocha et al.*, 2005]). We stress that the average effect of leads on  
39 climate can only be investigated by taking into account clouds, which would require a  
40 more detailed model than we used.

41 To estimate the impact of leads, a 1D atmospheric model coupled with a thermodynamic  
42 sea ice model is used. Lead-induced convective processes are represented similarly as  
43 in regional climate models, i.e., the heat emanated from leads is accounted for in the  
44 surface fluxes, but no details of the 3D interaction between convective plumes and their  
45 environment is modeled. Large-eddy simulations can provide more detailed information  
46 on the convection over leads, but our focus is on lead effects in climate and weather  
47 prediction models that cannot resolve convective plumes. We consider idealized scenarios  
48 (Section 3) with prescribed sea ice and open water (lead) fractions being typical for various  
49 regions of the polar oceans.

50 This study on the impact of leads differs from previous investigations with stand alone  
51 sea ice models as those of *Maykut and Untersteiner* [1971] and *Ebert and Curry* [1993].  
52 In their studies, 10-m wind and air temperature were taken from observations or from  
53 reanalyses. This procedure does not allow an independent ABL evolution, since the effect  
54 of leads on the forcing variables is not accounted for. This drawback is avoided here by  
55 prescribing only the geostrophic wind and sea ice fraction.

## 2. Model description

56 The atmospheric model is a 1D version of the model METRAS [*Schlünzen*, 1990]. Here,  
57 it is important to note that turbulent fluxes in the Ekman layer are determined as in

58 *Lüpkes and Schlünzen* [1996] with their nonlocal parameterization allowing countergra-  
59 dient transport of heat and humidity in case of convective conditions. A local mixing  
60 length closure is used at neutral and stable conditions [*Vihma et al.*, 2003]. Surface fluxes  
61 of momentum, latent and sensible heat are calculated separately for ice and water areas  
62 ( $F = AF_i + (1 - A)F_w$ , where  $A$  is the sea ice concentration,  $F_i$  and  $F_w$  are the surface  
63 fluxes over the ice-covered and open-water fractions). Stability functions of Dyer (1974)  
64 are used, but we limit the Obukhov length to 10 m for stable stratification. Roughness  
65 lengths for momentum are 1 mm and 0.1 mm over ice and water, respectively. The rough-  
66 ness length for heat is one tenth of it. Longwave atmospheric radiative cooling is taken  
67 into account prescribing a constant height dependent cooling rate according to *Vihma et*  
68 *al.* [2003]. The model is run with 34 layers, eight layers of which being below 200 m.

69 The sea ice model consists of 1D diffusion equations solved for the temperatures in the  
70 ice and snow layers. The equations are formulated following *Maykut and Untersteiner*  
71 [1971], *Ebert and Curry* [1993], and *Makshtas* [1998]. Empirical parameterizations are  
72 applied for longwave radiation fluxes with a constant value for the clear-sky emissivity for  
73 incoming longwave radiation. The model is run with 1 cm grid size. A sea ice thickness of  
74 2 m is prescribed. Sea ice is covered by a 30 cm snow layer typical for Arctic winter. Since  
75 we consider a winter situation and run the model only for a few days, melting effects are  
76 neglected. We assume that refrozen leads are replaced by new ones and that  $A$  remains  
77 constant. The water temperature in leads is also kept constant (271.35 K).

78 We initialize the model with a temperature profile typically observed over the central  
79 Arctic during the cold season, either when clouds prevent longwave radiative cooling of

80 the ABL or as a result of previous warm air advection from regions with less sea ice cover.  
81 The temperature profile is characterized by a shallow near-neutral boundary layer capped  
82 by a strong inversion at 100 m height. During a complete retreat of clouds we can expect  
83 rapid cooling of the sea ice surface and the atmospheric response will strongly depend  
84 on the amount of heat released from leads. Model results are generated for different  
85 geostrophic wind speeds prescribed to constant values during each run. The results are  
86 considered then as a function of the modeled 10-m wind speed at different output times.  
87 Results were similar for a prescribed fetch and choosing simulation times according to the  
88 ABL wind speed.

### 3. Results

89 The air and snow surface temperature after two days simulation time are shown in  
90 Figure 1 (bottom) for  $A = 95\%$  and  $A = 100\%$ . Temperatures are significantly lower  
91 than the initial 250 K, which is due to the radiative cooling. The modeled temperatures  
92 strongly depend on  $A$ . A decrease of  $A$  from 100 % to 95 % causes an increase of up to  
93 18 K ( $\approx 13$  K on average) in the 10-m potential temperature.

94 Two wind regimes exist with a separating wind speed  $v_s$  depending only slightly on  $A$   
95 ( $v_s = 4.5 \text{ m s}^{-1}$  for  $A = 95\%$  and  $v_s = 4 \text{ m s}^{-1}$  for  $A = 100\%$ ). In the strong-wind regime  
96 ( $v > v_s$ ) air and surface temperatures increase with increasing wind speed. This effect  
97 turns out to be independent on  $A$ , however, it is slightly more pronounced for complete  
98 ice cover. In the weak-wind regime ( $v < v_s$ ) the temperature dependence on wind speed  
99 differs from that in the strong-wind regime and the behavior of curves depends on  $A$ . For  
100  $A = 100\%$ , there is a decrease of air and surface temperature with increasing wind speed.

101 However, for  $A = 95$  % the surface temperatures behave as during strong wind, and the  
102 two regimes differ mainly by the stability. In the weak-wind regime the difference between  
103 the surface and 10-m air temperatures is after 2 days about 2-3 times larger than in the  
104 strong-wind regime. The stability in the weak-wind regime increases with decreasing  $A$ ,  
105 until a maximum is reached at about  $A = 50$  %, where the temperature difference reaches  
106 a value of 8 K (not shown). In the case of complete ice cover such large temperature  
107 differences do not occur. Hence, it is obvious that the heat emanating from open water is  
108 responsible for this stabilizing effect near the surface.

109 The role of leads becomes more clear by considering the energy fluxes compiled in Figure  
110 2 for  $A = 95$  %. In both wind regimes there is a significant upward sensible heat flux  
111 (Figure 2, top) originating from the leads. It is almost linearly increasing with increasing  
112 wind speed and compensated by the downward sensible heat flux over the ice areas.  
113 Obviously, most of the heat amount originating from leads is returned to the snow surface.  
114 Since the downward flux is larger at higher wind speeds, the snow surface temperature is  
115 also larger and the ABL temperature maintaining the equilibrium of upward fluxes over  
116 water and downward fluxes over ice is increasing as well (Figure 1). The energy budget  
117 at the snow surface can only be balanced by the aid of the conductive heat flux. This is  
118 important, especially in the weak-wind regime (Figure 2, bottom), where the snow surface  
119 is coldest and the temperature gradient through the ice and snow is therefore largest. At  
120  $v < v_s$  the downward sensible heat fluxes over ice are relatively small compared with  
121 the values for  $v > v_s$  and too small to prevent the snow surface from efficient cooling.

122 Therefore, ABL temperature and surface temperature appear to be decoupled to some  
 123 extent at weak wind (Figure 1).

124 In case of complete ice cover the effect of decoupling disappears, at least in the results  
 125 after two days simulation time, since the near-surface stabilizing effect caused by the heat  
 126 from leads is missing.

The decrease of air temperature with increasing wind in the weak-wind regime ( $A = 1.0$ ) can be explained with more efficient mixing at higher wind speeds, which leads to an increased loss of heat from the ABL to the surface. With increasing wind, also the snow temperature decreases as downward longwave radiation from the colder air is reduced. This holds only up to the threshold wind speed  $v_s$ . At larger wind speeds the increase of temperatures is caused by a growth of ABL thickness  $z_i$  (not shown). Its effect can be explained by considering the temperature equation integrated over  $z_i$ . Neglecting entrainment and radiation, we obtain

$$\frac{d\theta_m}{dt} = \frac{\overline{w'\theta'}|_s}{z_i},$$

127 where  $\theta_m$  represents the vertically averaged potential temperature in the ABL and  $\overline{w'\theta'}|_s$   
 128 is the surface heat flux. Hence, a strong increase of  $z_i$  decreases the ABL cooling caused  
 129 by downward flux of sensible heat. Further sensitivity studies demonstrated that this  
 130 effect is much stronger than that of entrainment.

131 Clear-sky conditions occur more often for time periods shorter than two days. Thus,  
 132 results are shown also after twelve hours of simulation (Figure 1, top). Here, the differences  
 133 between model runs with  $A = 100\%$  and  $A = 95\%$  are smaller, but still reach up to 7 K.  
 134 Furthermore, the decoupling effect between snow and atmosphere at low wind speeds is

135 more pronounced and occurs also for  $A = 100$  %. The reason is the initial rapid cooling  
136 of the surface and the too slow adjustment of ABL temperatures.

137 It is noteworthy that the minimum temperature of the snow surface is about 228 K  
138 after two days simulation time, a value, which is not far from the minimum temperature  
139 (229 K according to *Persson et al.* [2002]) observed during SHEBA. Figure 3 shows 10-m  
140 temperatures observed during SHEBA between December 1997 and February 1998 and  
141 modeled ones after two days for  $A = 99$  %. Detailed observations do not exist for a  
142 large region (corresponding to two days of air-mass advection) around the SHEBA site,  
143 but 99 % is a typical value for  $A$  in the central Arctic during winter. Since we consider  
144 clear-sky conditions, our study provides an estimation for extreme cases with the lowest  
145 temperatures. Hence, we have to compare the modeled curve with the lowest values for  
146 each wind speed during SHEBA. According to Figure 3 these lowest temperatures are well  
147 reproduced by the model. Furthermore, also during SHEBA two wind regimes exist with  
148 the separating wind speed at  $4 \text{ m s}^{-1}$ . Hence, the simple model fairly well represents the  
149 typical Arctic winter time situation during clear-sky conditions.

150 Figure 4 shows the modeled 10-m ABL temperatures as a function of prescribed  $A$ .  
151 Obviously, a small change of  $A$  has a strong impact on the ABL temperature. The curve  
152 steepens with increasing simulation time. A change of 1 % in  $A$  results in roughly 1 K and  
153 3.5 K change of the ABL temperature after 12 and 48 hours simulation time, respectively.

154 The sensitivity of results on atmospheric longwave radiative cooling was also tested.  
155 However, the structure of curves in Figures 1 and 4 remained unchanged. The new  
156 temperature curves were simply shifted parallel to the former ones.

#### 4. Discussion and conclusions

157 Obviously, there is a strong sensitivity of the results to the lead (or open water) fraction.  
158 The strong dependence of ABL temperature on the sea ice fraction demonstrates the need  
159 for very accurate observations of sea ice concentration  $A$  in the central polar regions.  
160 This generates a challenge for the development of remote sensing methods, since the  
161 present ones that can provide daily data with extensive spatial coverage are not accurate  
162 enough for  $A$  exceeding 90 % [e.g., *Andersen et al.*, 2007]. Furthermore, erroneous sea ice  
163 concentrations obtained from climate models could have a strong impact on their results.

164 Our results suggest that for  $A = 95$  % the upward sensible heat flux from leads practi-  
165 cally balances the downward flux over ice. Observations support this finding: *Overland et*  
166 *al.* [2000] draw analogous conclusions on the basis of analyses of SHEBA meteorological  
167 measurements and remote sensing data on the snow surface temperature in winter clear-  
168 sky conditions. We stress that the near-zero area-averaged heat flux is received via the  
169 significant lead effect on the ABL temperature.

170 Another important result consists of the existence of two wind regimes, which were  
171 modeled and also found in the SHEBA data. Our further sensitivity studies (not shown)  
172 revealed that the existence of the weak-wind regime depends on the surface layer stability  
173 function for stable stratification. E.g., stability functions allowing larger sensible heat  
174 fluxes directed to sea ice allow also a faster adjustment between air and snow surface  
175 temperature with a smaller value of  $v_s$ . Nevertheless, with the presently applied functions  
176 this adjustment was modeled earlier in good agreement to observations [*Vihma et al.*,  
177 2003]. Furthermore, decoupling of the atmosphere from the underlying surface at stable

178 stratification during low winds is a phenomenon often observed in polar regions e.g., over  
179 sea ice in the SHEBA experiment [*Grachev et al.*, 2005]. Our model results also suggest  
180 that the effect of leads in further stabilizing the lowest tens of meters of air over sea ice  
181 is important in maintaining the decoupling over periods of up to two days. This has not  
182 been addressed earlier.

183 The present estimations are valid for the polar night under clear-sky conditions. In  
184 overcast conditions over the Arctic sea ice the snow surface temperature is about 15 K  
185 warmer [*Vihma and Pirazzini*, 2005]. The surface temperature difference between leads  
186 and sea ice is accordingly strongly reduced, which dampens the lead effect on the ABL.

187 There are certainly additional factors influencing the ABL temperature, which were  
188 not considered so far. Besides clouds the most important one is horizontal advection.  
189 It may overlay the considered cooling/heating rates and should be included into future  
190 investigations. Finally, the results depend also on the initial conditions, on parameters like  
191 sea ice thickness, snow thickness, surface roughness, and the prescribed initial boundary  
192 layer depth. However, it turned out from additional model runs that the variation of all  
193 these parameters hardly changes our conclusions.

194 **Acknowledgments.** This study was supported by the EU project DAMOCLES (grant  
195 no. 18509), which is part of the Sixth Framework Programme, by DFG (grant no. LU  
196 818/1-1) and by the Academy of Finland (grant 210794). Observations shown in Figure 3  
197 were made by the SHEBA Atmospheric Surface Flux Group, Ed Andreas, Chris Fairall,  
198 Peter Guest, and Ola Persson.

## References

- 199 Arctic Climate Impact Assessment (ACIA) (2005), Chapter 6: Cryosphere and Hydrology,  
200 John E. Walsh et al., Cambridge University Press, www.acia.uaf.edu, 184–236.
- 201 Curry, J., Schramm, J.L., Serreze, M.C., and E.E. Ebert (1995), Water vapor feedback  
202 over the Arctic ocean, *J. Geophys. Res.*, 100(D7), 14,223–14,229.
- 203 Dyer, A.J. (1974), A review of flux-profile relationship, *Boundary-Layer Meteorol.*, 7,  
204 363–372.
- 205 Ebert, E.E., and J.A. Curry (1993), An intermediate one-dimensional thermodynamic  
206 sea ice model for investigating ice-atmosphere interactions, *J. Geophys. Res.*, 98(C6),  
207 10085–10109.
- 208 Grachev, A.A., Fairall, C.W., Persson, P.O.G., Andreas, E.L., and P.S. Guest (2005),  
209 Stable boundary-layer regimes: The SHEBA data, *Boundary-Layer Meteorol.*, 116, 201-  
210 235.
- 211 Lüpkes, C. and K.H. Schlünzen (1996), Modelling the Arctic convective boundary-layer  
212 with different turbulence parameterizations, *Boundary-Layer Meteorol.*, 79, 107–130.
- 213 Makshtas, A.P. (1998), Thermodynamics of sea ice, in *Physics of ice-covered seas*, edited  
214 by M. Leppäranta, pp. 289-303, University Printing House, Helsinki.
- 215 Maykut, G.A., and N. Untersteiner (1971), Some results from a time dependent thermo-  
216 dynamic model of sea ice, *J. Geophys. Res.*, 76(6), 1550–1575.
- 217 Mirocha, J.D., Kosovic, B., and J. Curry (2005), vertical heat transfer in the lower atmo-  
218 sphere over the Arctic ocean during clear-sky periods, *Boundary-Layer Meteorol.*, 117,  
219 37–71.

- 220 Overland, J. E., McNutt, S. L., Groves, J., Salo, S., Andreas, E. L., and P. O. G. Persson  
221 (2000), Regional sensible and radiative heat flux estimates for the winter Arctic during  
222 the Surface Heat Budget of the Arctic Ocean (SHEBA) experiment, *J. Geophys. Res.*,  
223 105 (C6), 14093–14102.
- 224 Schlünzen, K. H. (1990), Numerical studies on the inland penetration of sea breeze fronts  
225 at a coastline with tidally flooded mudflats, *Beitr. Phys. Atmosph.*, 63, 243–256.
- 226 Sorteberg, A., Kattsov, V., Walsh, J.E., and T. Pavlova (2007), The Arctic surface energy  
227 budget as simulated with the IPCC AR4 AOGCMs, *Clim. Dyn.*, 29, 131–156.
- 228 Vihma, T., Hartmann, J. and C. Lüpkes (2003), A case study of an on-ice air flow over  
229 the Arctic marginal sea ice zone, *Boundary-layer Meteorol.*, 107,189–217.
- 230 Vihma, T., and R. Pirazzini (2005), On the factors controlling the snow surface and 2-m  
231 air temperatures over the Arctic sea ice in winter, *Boundary-layer Meteorol.*, 117,73–90.

## 5. Figures

232 **Figure 1:** Modeled snow surface temperature (blue) and 10-m air potential temperature  
233 (red).

234

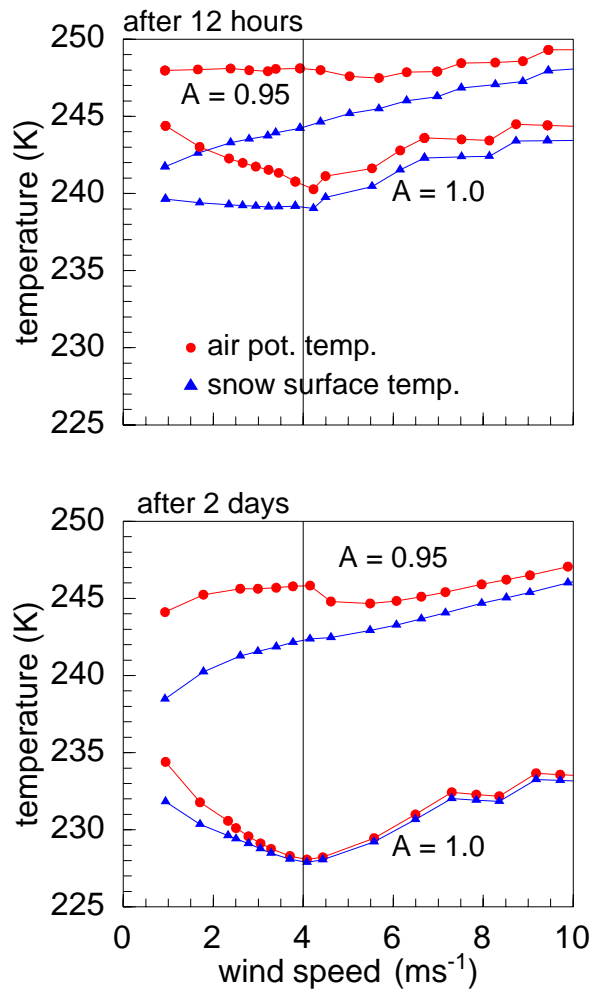
235 **Figure 2:** Top: area averaged surface fluxes in the atmosphere model for  $A = 95\%$   
236 after two days simulation time. Bottom: fluxes in the snow/ice model related only to the  
237 ice covered area (downward fluxes are negative).

238

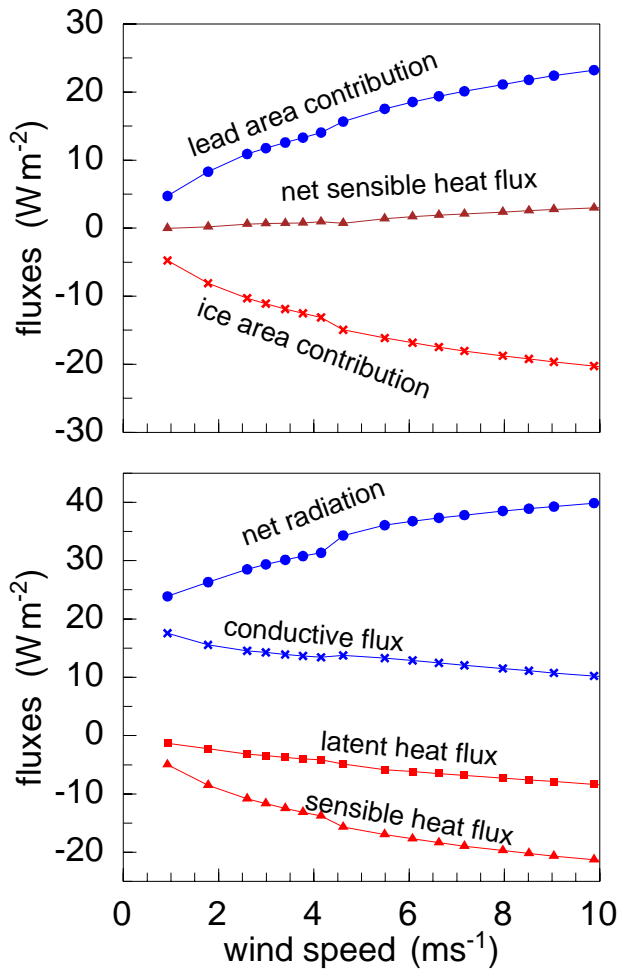
239 **Figure 3:** 10-m air temperature observed during SHEBA between December 1997 and  
240 February 1998 (black symbols) and model results for  $A = 99\%$  after two days (blue).

241

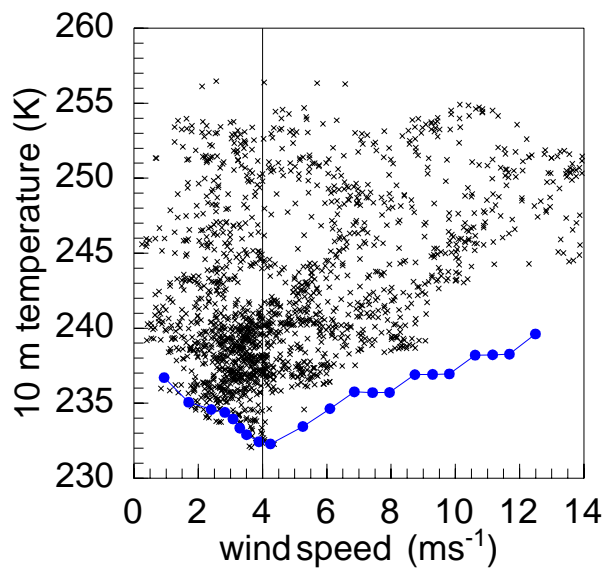
242 **Figure 4:** Model results after 12 hours (open symbols) and after two days (closed sym-  
243 bols) simulation time.



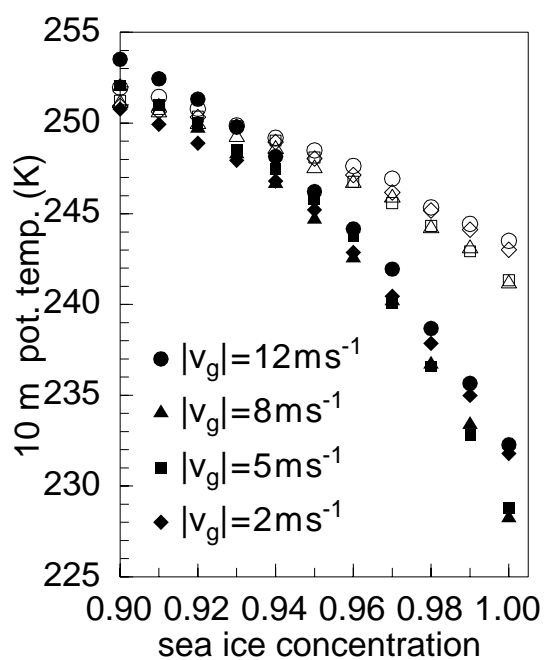
244 Fig. 1



245 Fig. 2



246 Fig. 3



247 Fig. 4